A Highly Efficient and Reliable Inverter Configuration Based Cascaded Multi-Level Inverter for PV Systems

Sachin Jain, *Senior Member, IEEE* and Venu Sonti, *Student Member, IEEE*

Abstract—**This paper presents an improved Cascaded Multi-Level Inverter (CMLI) based on a highly efficient and reliable configuration for the minimization of the leakage current. Apart from a reduced switch count, the proposed scheme has additional features of low switching and conduction losses. The proposed topology with the given PWM technique reduces the high-frequency voltage transitions in the terminal and common-mode voltages. Avoiding high-frequency voltage transitions achieves the minimization of the leakage current and reduction in the size of EMI filters. Furthermore, the extension of the proposed CMLI along with the PWM technique for *2m+1* levels is also presented, where *m* represents the number of Photo Voltaic (PV) sources. The proposed PWM technique requires only a single carrier wave for all *2m+1* levels of operation. The Total Harmonic Distortion (THD) of the grid current for the proposed CMLI meets the requirements of IEEE 1547 standard. A comparison of the proposed CMLI with the existing PV Multi-Level Inverter (MLI) topologies is also presented in the paper. Complete details of the analysis of PV terminal and common-mode voltages of the proposed CMLI using switching function concept, simulations, and experimental results are presented in the paper.**

Index Terms—**Cascaded multi-level inverter, leakage current, common-mode voltage, terminal voltage.**

I. INTRODUCTION

TRANSFORMERLESS Multi-Level Inverter (MLI) topologies are gaining importance due to their advantages such as high efficiency, low switch count, low weight and reduced size. However, removal of the transformer eliminates the galvanic isolation between the PV array and the output load. Removal of galvanic isolation increases the leakage current compromising the safety in PV systems. It has led to the development of various safety standards for the PV systems, which restrict the value or magnitude of leakage current flow in the PV system [1-5]. Apart from leakage current minimization, there is a continuously increasing demand for high-quality power output to be fed into the grid

Sachin Jain and Venu Sonti are with the Department of Electrical Engineering, National Institute of Technology, Warangal, Telangana – (506004) INDIA. (e-mail:jsachin@nitw.ac.in,venu312@nitw.ac.in).

from the PV system. This requirement has led to the use of multi-level inverters (MLI) in the transformerless PV systems. In literature, many topologies or configurations of MLIs [6-7] are proposed for the minimization of leakage current for their application in the transformerless PV systems. These configurations employ two methods for minimization of the leakage current [8]. One method is based on maintaining the common-mode voltage (CMV) constant, while the other method is based on the minimization of the high-frequency transitions in the terminal and common-mode voltages.

One elegant solution based on maintaining a constant CMV is proposed by Zhang *et al.* [9]. The given MLI configuration [9] consists of eight switches for the generation of three levels in the output voltage. This topology reduces the switching losses but has the drawback of high conduction losses during both turn-ON and zero voltage states. The given MLI configuration has an asymmetric operation during each half-cycle of the fundamental component of the grid voltage. The inherent asymmetry in each half-cycle causes a DC offset in the MLI output voltage. Furthermore, the requirement of an additional number of switches for more than three-level operation limits its application. Islam *et al.* [10] have proposed another interesting transformerless PV MLI topology to reduce the leakage current by maintaining CMV constant. This MLI topology uses six switches for the generation of three levels in the inverter output voltage. This circuit configuration results in high switching and conduction losses. Furthermore, this MLI topology cannot be extended to more than three levels in the output voltage. Xiao *et al.* [11] have proposed another efficient three-level MLI for the minimization of leakage current by maintaining CMV constant. The given topology [11] has low conduction and switching losses. However, this configuration suffers from the disadvantage of a high number of device count. Another interesting topology with low switching losses based on constant CMV is proposed by Ji *et al.* [12]. This MLI topology consists of six switches and two diodes. Apart from resulting in high conduction losses, this topology is less amenable for an extension to a higher number of levels in the output voltage.

Another important method to minimize the leakage current is by the elimination of high-frequency voltage transitions in the CMV. One such interesting solution is proposed by Buticchi *et al.* [13]. The authors have proposed a nine-level grid-tied PV MLI topology. This MLI topology consists of eleven switches and four diodes. In this MLI, four switches in the low voltage bridge are operated with high switching

frequency, while the remaining switches in the high voltage bridge are operated with the low switching frequency. For a proper operation of this configuration [13], the balance of flying capacitor voltage V_{fc} is necessary. Furthermore, the PV terminals in this MLI topology cannot be grounded. Based on a similar concept, another good proposal is given by Hong *et al.* [14]. In this solution, the authors have proposed single inductor dual buck full-bridge inverter for the generation of variable CMV at low-frequency. The MLI topology requires six switches and two diodes. The switches in the H-bridge are operated at a low switching frequency, while the bi-directional switch is operated at a high switching frequency. However, details of extending the topology for a higher number of levels is not explained in the paper [14].

From the above discussion, it is evident that there is a need for a generalized transformerless PV MLI, with fewer semiconductor devices to achieve the objectives of high efficiency and economy. It should also be ensured that the PV MLI should have its switching and conduction losses optimized with a lower number of conducting switches during the zero voltage state. Furthermore, the extension to the higher number of levels should be possible. This paper proposes one such solution for the minimization of leakage current in transformerless MLIs connected to PV systems. The pulse width modulation (PWM) technique for the proposed MLI is also discussed in the paper. The analysis of PV terminal and common-mode voltages using switching function is presented. This analysis leads to the development of the proposed PWM technique, which prevents high-frequency voltage transitions in the terminal voltage and CMV. Salient features of the proposed cascaded multilevel inverter (CMLI) are:

1) The topology uses eight switches for the generation of five levels in the output voltage.
2) During the zero voltage state only one switch and one diode conduct.
3) In the proposed topology, four switches are operated at a low switching frequency, which reduces the switching losses.
4) The dead band in PWM technique does not affect the common-mode voltage.
5) The proposed inverter can be easily cascaded to achieve more than five levels in the output.

Rest of the manuscript is organized into eight sections. Section II describes the working principle and the operation for the proposed five-level grid-connected CMLI along with the generalized structure. The details of the PWM technique employed with its generalization for *2m+1* levels are explained in section III. Section IV gives the details of the Maximum Power Point Tracking (MPPT) algorithm which can be applied to the proposed five-level CMLI. This is followed by the analysis of terminal and common-mode voltages for the proposed CMLI in section V. Section VI discusses the simulation results of the proposed five-level grid-connected CMLI. Section VII shows the experimental results of the proposed five-level and nine-level CMLI. Comparison of the proposed CMLI with the other existing PV MLI topologies in the literature is presented in section VIII. The conclusions from the paper are discussed in section IX.

II. OPERATION OF PROPOSED CASCADED FIVE-LEVEL MLI

The schematic circuit diagram of the proposed five-level CMLI for PV system is shown in Fig. 1. The given configuration consists of two converters (Conv-1 and Conv-2). Conv-1 is a half-bridge inverter comprising two switches S_{x1} and S_{x2}. The Conv-2 comprises of a highly efficient and reliable inverter configuration [15] with six switches (S_{x3} to S_{x8}). Among the six switches, four switches (S_{x3} to S_{x6}) in Conv-2 constitute an H-bridge circuit. The remaining two switches S_{x7} and S_{x8} in Conv-2 are bi-directional switches. The switches in the Conv-1 are used to generate the voltage levels of V_{PV} and $V_{PV}/2$. When switch S_{x1} is turned ON, the voltage V_{PV} is applied at the terminal n with respect to the terminal z. Similarly, the terminal n attains the voltage $V_{PV}/2$ when switch S_{x2} is turned ON. The switches S_{x1} and S_{x2} are complementary in nature. The generated voltage levels at the terminal n of Conv-1 are given as an input to the Conv-2. The Conv-2 generates the positive, negative and zero levels of corresponding input voltage (voltage between the terminals n and z) across the load. The bi-directional switches S_{x7} and S_{x8} provide the free-wheeling path during zero voltage state. The output of the five-level CMLI is connected to the grid through an LCL filter as shown in Fig. 1 [16-18]. It consists of inverter side inductance L_i, capacitance C_f and grid side inductance L_{ac}. The resistance R_d in the shunt branch of the filter is used as a damping resistor. The resistance R_{ac} refers to the grid side resistance, and the resistance R_g indicates resistance in the ground path. The variable v_{ac} refers to instantaneous grid voltage. The variables R_p and C_p refer to the parasitic resistance and capacitance in the PV system, respectively shown with dotted lines in Fig. 1. The parasitic capacitance in PV system forms a resonant circuit with the filter inductances [16]. The variables i_o, i_c and i_{ac} denote the output current of five-level CMLI, current flowing through shunt branch of the filter and the current flowing into the grid respectively. The current i_{leak} indicates the leakage current flowing from the PV array into the ground through parasitic capacitance (see Fig. 1).

The proposed MLI topology contains four pairs of complementary switches (S_{x1}, S_{x2}), (S_{x3}, S_{x4}), (S_{x5}, S_{x6}) and (S_{x7}, S_{x8}) in the proposed configuration. However, to minimize the leakage current, the complementary switching is employed only for the two pairs of switches (S_{x1}, S_{x2}) and (S_{x7}, S_{x8}).
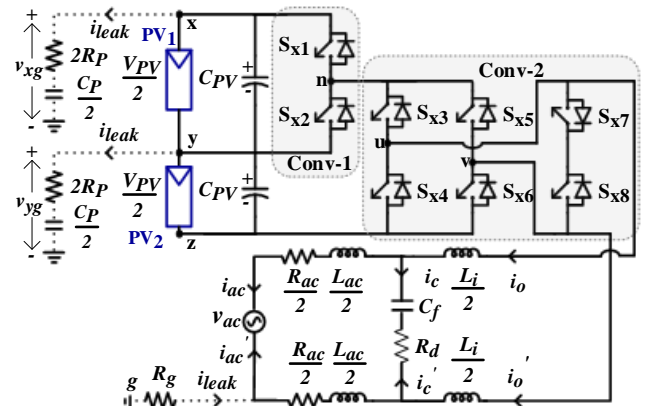

Fig. 1. Proposed five-level grid-connected CMLI with PV and parasitic elements.

Avoiding complementary action for the other pairs of switches helps in isolating the PV and the grid source during zero voltage state.

Fig. 2 shows the operation of the inverter in all its switching states. The inverter output voltage v_{uv} at different voltage levels with the corresponding switching states of all the switches are shown in Table I. The inverter output voltage v_{uv} attains the voltage levels $+V_{PV}$ or $-V_{PV}$ when switch S_{x1} is turned ON along with other inverter switches (S_{x3}, S_{x6}) or (S_{x4}, S_{x5}) respectively as shown in Figs. 2(a) and 2(e). Similarly, the the voltage levels $+V_{PV}/2$ or $-V_{PV}/2$ are obtained at v_{uv} when switch S_{x2} is turned ON with the same switching combinations as shown in Figs. 2(b) and 2(d). The most important feature to be noticed during zero voltage state or free-wheeling stage is the isolation or disconnection between PV source and the grid. The isolation between the PV source and the grid can be achieved by turning OFF all the switches of H-bridge inverter as shown in Fig. 2(c).

The turn-OFF state of four switches in H-bridge during zero voltage state results in the isolation of PV source from the grid. The bi-directional switches S_{x7} and S_{x8} provide a free-wheeling path for the inductor current during the turn-OFF period of a switching cycle. This action helps in minimizing the leakage current flowing through the parasitic capacitance. As there is no direct connection between the two sources, the PV terminal points (nodes x, y and z) float and have undefined voltages. The float or undefined value restricts the terminal voltages from becoming zero. Thus, high-frequency voltage transitions at the PV terminals are avoided. In other words, the possibility of the flow of leakage current can be minimized. Also, in the other intermediate states like switching between $V_{PV}/2$ to V_{PV} or vice-versa, again the same principle can be used. The above action further helps in the minimization of the leakage current in the PV system. The PWM technique for the proposed five-level CMLI is broadly discussed in section III. The expression for the pole voltages v_{uz} and v_{vz} are given in (1) and (2) respectively.
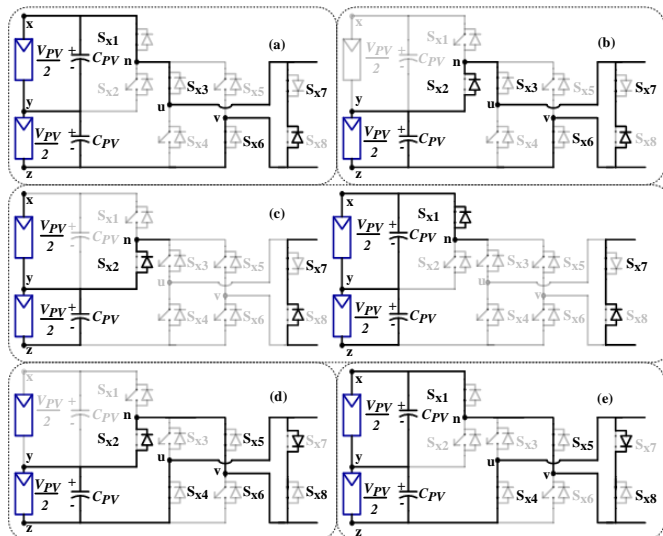
TABLE I
SWITCHING STATES WITH THEIR RESPECTIVE OUTPUT VOLTAGE

S_{x1}	S_{x2}	S_{x3}	S_{x4}	S_{x5}	S_{x6}	S_{x7}	S_{x8}	v_{uv}
1	0	1	0	0	1	1	0	$+V_{PV}$
0	1	1	0	0	1	1	0	$+V_{PV}/2$
0	1	0	0	0	0	1	0	0
1	0	0	0	0	0	1	0	0
0	1	0	1	1	0	0	1	$-V_{PV}/2$
1	0	0	1	1	0	0	1	$-V_{PV}$

$$v_{uz} = \left(S_1 S_3 + 0.5 S_2 S_3 - \frac{1}{(S_3 + S_4)} + \frac{1}{(S_3 + S_4)(S_1 + S_2)} \right) V_{PV} \quad (1)$$

$$v_{vz} = \left(S_1 S_5 + 0.5 S_2 S_5 - \frac{1}{(S_5 + S_6)} + \frac{1}{(S_5 + S_6)(S_1 + S_2)} \right) V_{PV} \quad (2)$$

where S_a, (a=1, 2, 3...) is the switching state of switch S_{xa} whose value can be either 1 (stands for turn-ON) or 0 (stands for turn-OFF) respectively.

Fig. 3 shows the switching pattern of all the switches for the corresponding inverter output voltage v_{uv}. The switches S_{x1} and S_{x2} in the half-bridge are operated at low switching frequency. In order to eliminate the high switching frequency operation, the switch S_{x2} is kept turned ON in zero state during voltage transition between the levels 0 to $V_{PV}/2$. Similarly, the switch S_{x1} is kept turned ON, during voltage transition between levels 0 to V_{PV}. The inverter switch pair (S_{x3}, S_{x6}) is operated with a high switching frequency during positive half-cycle, and it remains at the turn-OFF state during the negative half-cycle of the inverter output voltage v_{uv}. A similar operation is applicable to the other inverter switch pair (S_{x4}, S_{x5}), which is operated with higher switching frequency during the negative half-cycle.

The switches S_{x7} and S_{x8} are turned ON during positive and negative half cycles of the output voltage v_{uv} respectively. The removal of complementary action from the pair of switches (S_{x3}, S_{x4}) and (S_{x5}, S_{x6}) facilitates complete turn-OFF of the switches during each half-cycle of the output voltage v_{uv}. Thus, the proposed system has the advantage of reduced switching losses, realizing to a highly efficient and reliable inverter configuration which may result in higher efficiency.

The generalized topology for $2m+1$ levels can also be obtained for the proposed five-level CMLI. The number of PV sources in CMLI is denoted by the term m. The value of m is always an integral multiple of 2 (i.e., m =2, 4…). The extended version of the proposed CMLI for $2m+1$ levels is presented in Fig. 4. The generalized topology is obtained by cascading the basic units consisting of half-bridge and H-bridge. The bi-directional switches are connected in between the output terminals for the free-wheeling period. The proposed generalized $2m+1$ level MLI is also compared with the half-bridge and full-bridge modular multi-level converter. The half-bridge modular multi-level converter requires less number of switches when compared to the proposed generalized $2m+1$ level MLI. However, it is difficult to reduce or minimize the flow of leakage current in the half- bridge modular multi-level converter. Also, the number of electrolytic capacitors used at the input side of the half-bridge

Fig. 2. Single Phase five-level cascaded MLI for output voltage levels (a) $+V_{PV}$ (b) $+V_{PV}/2$ (c) 0 (d) $-V_{PV}/2$ (e) $-V_{PV}$.
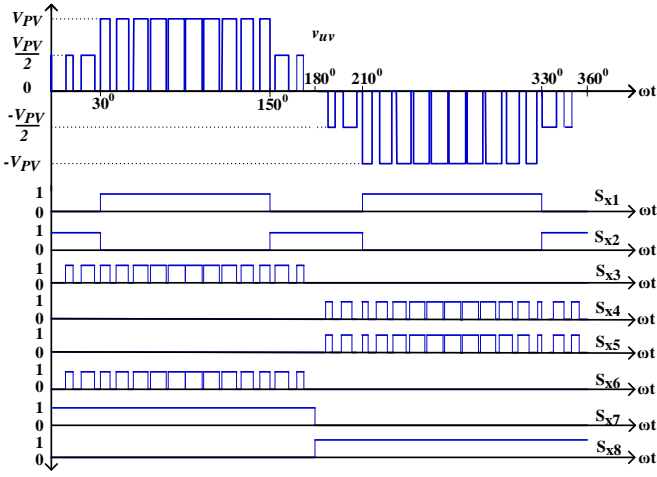
Fig. 3. Gate pulses for the switches corresponding to inverter output voltage.

modular multi-level converter is high compared to the proposed generalized *2m+1* level MLI. The proposed MLI has a lesser device count when compared to the full-bridge modular multi-level converter [19]. However, both can minimize the leakage current flowing through the PV system.

III. PROPOSED PWM STRATEGY ALONG WITH GENERALIZED STRATEGY FOR MINIMIZATION OF THE LEAKAGE CURRENT

The operation of the proposed PWM technique is explained by considering the given five-level CMLI. The high-frequency transitions in the terminal voltages v_{xg} and v_{yg} of five-level CMLI are minimized using the proposed PWM technique. The suggested action can be achieved by switching from V_{PV} to 0 state or vice-versa instead of the switching from V_{PV} to $V_{PV}/2$ state or vice-versa. Additionally, during the zero voltage state or free-wheeling period of the switching cycle, the PV array is isolated from the grid. The isolation of the PV array and the grid during zero voltage state is similar to the inverter configuration reported in [15]. The magnitude of reference wave v_{mod} is lowered to 50% of its original value whenever the switching is toggled amongst the levels V_{PV} and 0. The above action is mainly done to accommodate the value of PV voltage V_{PV}. The modification in the value of v_{mod} is done whenever the
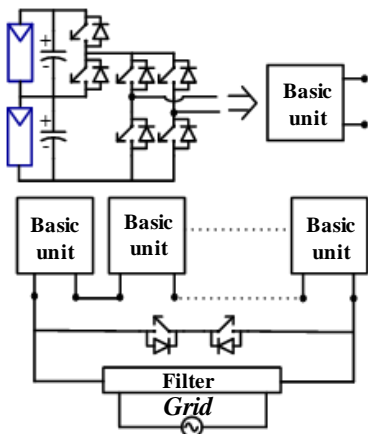

Fig. 4. Generalized *2m+1* level MLI topology derived from proposed five-level CMLI.

instantaneous magnitude of modulating wave v_{mod} exceeds the value of $m_a/2$, where m_a refers to the modulation index. By incorporating the desired modification, the output voltage includes the zero voltage state (i.e., free-wheeling state) in all its switching periods. The expression for modified reference waveform $v_{ref\_modified}$ is given in (3).

$$v_{ref\_modified} = \begin{cases} v_{mod} & for \quad 0 \leq |v_{mod}| < \dfrac{m_a}{2} & from \quad \dfrac{V_{PV}}{2} to \ 0 \\ \dfrac{v_{mod}}{2} & for \quad \dfrac{m_a}{2} \leq |v_{mod}| < m_a & from \ V_{PV} \ to \quad 0 \end{cases} \quad (3)$$

where, $v_{mod} = m_a \sin\omega t$ gives the magnitude of v_{mod}.

The output voltage of the proposed PWM technique for the five-level CMLI is shown in Fig. 5. In Fig. 5 the modified reference wave is compared with the triangular carrier wave. During the positive half-cycle of voltage v_{ac}, whenever the phase angle ωt lies in range 0^0 to 30^0 and the instantaneous magnitude of $v_{ref\_modified}$ exceeds the carrier wave, then v_{uv} attains the voltage level of $V_{PV}/2$ otherwise, it is switched zero voltage state. Similarly, when ωt lies in the range 30^0 to 150^0, the inverter output voltage v_{uv} attains the voltage level of V_{PV} whenever the instantaneous magnitude $v_{ref\_modified}$ exceeds the carrier wave or attains zero value otherwise. In the same positive half-cycle, for the remaining range of ωt (i.e., between 150^0 to 180^0), v_{uv} attains the voltage levels $V_{PV}/2$ if the instantaneous magnitude of $v_{ref\_modified}$ is greater than the carrier wave. A similar sequence is adopted during the negative half-cycle of voltage v_{ac}. Thus, in the complete cycle if the magnitude of $v_{ref\_modified}$ is less than the carrier wave, then v_{uv} attains zero voltage level.

For the implementation of the proposed PWM to a *2m+1* level inverter, the waveform of generalized modified reference wave $v_{ref\_modified\_gen}$ is shown in Fig. 6. The term m refers to the number of PV sources used. Whenever the instantaneous absolute magnitude of v_{mod} exceeds the value $j(m_a/m)$, the magnitude of $v_{ref\_modified\_gen}$ becomes $k(|v_{mod}|/m)$ where $j = 1, 2,\dots m-1, m$ and $k = 1, 2, \dots m-1$. The expression for the $v_{ref\_modified\_gen}$ is given in (4).
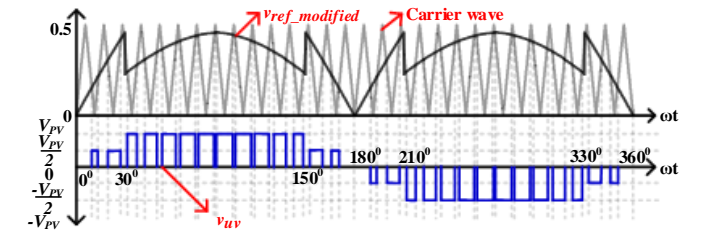

Fig. 5. The waveform of output voltage v_{uv} for the proposed PWM technique.

$$v_{ref\_modified\_gen} = \begin{cases} v_{mod} & for \quad 0 \leq |v_{mod}| < \dfrac{m_a}{m} & from \ \dfrac{V_{PV}}{m} to \ 0 \\ \dfrac{v_{mod}}{2} & for \quad \dfrac{m_a}{m} \leq |v_{mod}| < \dfrac{2m_a}{m} & from \ \dfrac{2V_{PV}}{m} to \ 0 \\ & . \\ & . \\ \dfrac{v_{mod}}{m} & for \quad \dfrac{(m\text{-}1)m_a}{m} \leq |v_{mod}| < m_a & from \ V_{PV} \ to \quad 0 \end{cases} \quad (4)$$

IV. INTEGRATION OF MPPT FOR PROPOSED FIVE-LEVEL CMLI

The well-known perturb and observe algorithm[20] is employed for the two PV sources (considering five-level
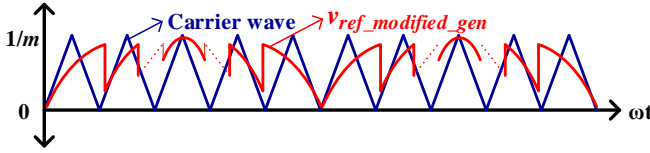
Fig. 6. The waveform of generalized modified reference wave $v_{ref\_modified\_gen}$.

operation) individually to track Maximum Power Point (MPP). Thus, each MPPT algorithm tracks the MPP for respective PV sources. To track the MPP, the required information of (i) the average values of the two PV source voltages (V_{PV1} and V_{PV2} for the PV sources PV_1 and PV_2 respectively) and (ii) the currents (I_{PV1} and I_{PV2} for the PV sources PV_1 and PV_2 respectively) are sensed and then given to their respective MPPT algorithms. The MPPT algorithms then use the sensed values of the PV voltages and currents for the calculation of the individual values of the modulation indices m_{a1} and m_{a2} for the two PV sources PV_1 and PV_2 respectively. The outputs of two MPPT algorithms are then utilized for the calculation of overall modulation index m_a. The expression for m_a is given in (5).

$$m_a = m_{a1} \frac{V_{PV1}}{V_{PV1}+V_{PV2}} + m_{a2}\frac{V_{PV2}}{V_{PV1}+V_{PV2}} \quad (5)$$

The calculated modulation index m_a is then used by the PWM strategy as described in the above section to generate the PWM pulses for the proposed five-level CMLI.

V. ANALYTICAL EXPRESSIONS OF PV TERMINAL VOLTAGE AND COMMON-MODE VOLTAGE FOR PROPOSED CASCADED FIVE-LEVEL INVERTER

The analysis of the leakage current can be carried out from the expression of terminal voltages v_{xg}, v_{yg} and v_{zg}. The expression for the PV terminal voltages can be derived from switching function analysis [21]. From Fig. 1, using the superposition theorem, the PV terminal voltages v_{xg} and v_{yg} are expressed as follows:

$$v_{xg} = S_1 v_{x1g} + S_2 v_{x2g} \quad (6)$$

$$v_{yg} = S_1 v_{y1g} + S_2 v_{y2g} \quad (7)$$

The terms v_{x1g} and v_{y1g} are the voltages at terminals x and y respectively when switch S_{x1} is turned ON. Similarly, v_{x2g} and v_{y2g} are the voltages at terminals x and y respectively when switch S_{x2} is turned ON.
The expression for the voltage v_{zg} when switch S_{x1} is turned ON is given in (8).

$$v_{zg} = v_{x1g} - V_{PV} \quad (8)$$

Similarly, the expression for terminal voltage v_{zg} when switch S_{x2} is turned ON is given in (9).

$$v_{zg} = v_{y2g} - \frac{V_{PV}}{2} \quad (9)$$

With the use of switching function analysis, the voltages v_{ug} and v_{vg} (from Fig. 1 and Fig. 2) expressed in terms of v_{x1g} and v_{zg} are shown in (10) and (11) respectively.

$$v_{ug} = S_1 S_3 v_{x1g} + S_4 v_{zg} \quad (10)$$

$$v_{vg} = S_1 S_5 v_{x1g} + S_6 v_{zg} \quad (11)$$

Similarly, the voltages v_{ug} and v_{vg} (from Fig. 1 and Fig. 2) expressed in terms of v_{y2g} and v_{zg} using switching functions are shown in (12) and (13) respectively.

$$v_{ug} = S_2 S_3 v_{y2g} + S_4 v_{zg} \quad (12)$$

$$v_{vg} = S_2 S_5 v_{y2g} + S_6 v_{zg} \quad (13)$$

Now expressing the voltages v_{ug} and v_{vg} in terms of the grid voltage v_{ac}, the voltage drop in filter inductors (L_i and L_{ac}) and resistances (R_{ac} and R_g) [21] can be given by:

$$v_{ug} = \frac{L_i}{2}\frac{di_o}{dt} + \frac{L_{ac}}{2}\frac{di_{ac}}{dt} + v_{ac} + \frac{R_{ac}}{2}i_{ac} - R_g i_{leak} \quad (14)$$

$$v_{vg} = \frac{L_i}{2}\frac{di_o{'}}{dt} + \frac{L_{ac}}{2}\frac{di_{ac}{'}}{dt} + \frac{R_{ac}}{2}i_{ac}{'} - R_g i_{leak} \quad (15)$$

Now with the addition of (14) and (15), and by ignoring the voltage drop in resistances R_g and $R_{ac}/2$ with assumptions of $i_{ac}=-i_{ac}{'}$ and $i_o=-i_o{'}$, [21] gives:

$$v_{ug} + v_{vg} = v_{ac} \quad (16)$$

Substituting the values of v_{ug} and v_{vg} from (10) and (11) in (16) and simplifying those using (8) gives the expression for the terminal voltage v_{x1g} in (17).

$$v_{x1g} = \frac{v_{ac} + V_{PV}\left(S_4 + S_6\right)}{\left(S_1 S_3 + S_1 S_5 + S_4 + S_6\right)} \quad (17)$$

Now, the other terminal voltage v_{y1g} (when switch S_{x1} is ON) can be calculated by subtracting v_{x1g} and $V_{PV}/2$.
Similarly, substituting (12) and (13) in (16) and simplifying for terminal voltage v_{y2g} using (9) results in (18).

$$v_{y2g} = \frac{v_{ac} + \frac{V_{PV}}{2}\left(S_4 + S_6\right)}{\left(S_2 S_3 + S_2 S_5 + S_4 + S_6\right)} \quad (18)$$

The other terminal voltage v_{x2g} can be calculated by adding v_{y2g} and $V_{PV}/2$. Now by using (6) and (7), the complete expression for terminal voltages v_{xg} and v_{yg} is given in (19) and (20) respectively.

$$v_{xg} = v_{ac}S_{W1} + V_{PV}S_{W2} + v_{ac}S_{W3} + \frac{V_{PV}}{2}S_{W4} + \frac{V_{PV}}{2}S_2 \quad (19)$$

$$v_{yg} = v_{ac}S_{W1} + V_{PV}S_{W2} + v_{ac}S_{W3} + \frac{V_{PV}}{2}S_{W4} - \frac{V_{PV}}{2}S_1 \quad (20)$$

The terms S_{W1}, S_{W2}, S_{W3} and S_{W4} in (19) and (20) are given by,

$$S_{W1} = \frac{S_1}{\left(S_1 S_3 + S_1 S_5 + S_4 + S_6\right)} \qquad S_{W2} = \frac{S_1(S_4 + S_6)}{\left(S_1 S_3 + S_1 S_5 + S_4 + S_6\right)}$$

$$S_{W3} = \frac{S_2}{\left(S_2 S_3 + S_2 S_5 + S_4 + S_6\right)} \qquad S_{W4} = \frac{S_2(S_4 + S_6)}{\left(S_2 S_3 + S_2 S_5 + S_4 + S_6\right)}$$

Substituting the values $S_3=0$, $S_4=0$, $S_5=0$ and $S_6=0$ in the voltage state result in undefined value (0/0) in the terminal voltages v_{xg}, v_{yg} and v_{zg}. The undefined value (0/0) during a zero voltage state is mainly because of isolating the PV source and grid. The isolation of PV source and grid can also be

observed in Fig. 2(c). The common-mode voltage v_{cm} is obtained by taking the average of pole voltage v_{uz} and v_{vz} given in (1) and (2) respectively. The expression for the v_{cm} is expressed in (21).

$$v_{cm} = \left(\left(S_1 + 0.5S_2 \right) \left(S_3 + S_5 \right) + \left(\frac{1}{\left(S_3 + S_4 \right)} + \frac{1}{\left(S_5 + S_6 \right)} \right) \left(\frac{1}{\left(S_1 + S_2 \right)} - 1 \right) \right) \frac{V_{PV}}{2}$$

(21)

Table II gives the values of pole voltages (v_{uz}, v_{vz}) and common-mode voltage v_{cm} at different levels in the output voltage v_{uv}. During the turn-OFF period in a switching cycle, all the switches in the H-bridge are in a cut-off state so that the switching states S_3, S_4, S_5 and S_6 are equal to zero value. Substituting the corresponding values of S_3, S_4, S_5, S_6 in (21) results in an undefined value (i.e., v_{cm}= 0/0) during the zero voltage state. The common-mode voltage attains the value $V_{PV}/2$ for both positive and negative levels of output voltage V_{PV} and attains the value $V_{PV}/4$ for both positive and negative levels of output voltage $V_{PV}/2$.

The expressions for terminal and common-mode voltages can be verified with MATLAB software using simulink block-set. The parameters V_{PV} =400V, switching frequency of the carrier wave f_{sw} =1kHz, v_{ac}= 220V (RMS) and the grid frequency f_g = 50Hz are considered for the simulation. The carrier wave frequency is restricted to 1kHz. This is done to demonstrate the undefined states clearly. Fig. 7 shows the waveforms of terminal voltages v_{xg}, v_{yg}, v_{zg} and common-mode voltage v_{cm}. The discontinuity in the waveforms occurs when the PV source and grid are isolated. The isolation of grid and PV array results in an undefined value in the terminal and common-mode voltages (discontinuity in the waveform). Since the value of the terminal and common-mode voltages is undefined during the zero voltage state, they can be assumed to be restricted to the previous value. Thus, transitions in the voltage waveform can be minimized. In other words, it results in minimizing the high-frequency voltage transitions in the terminal and common-mode voltages. Minimization or reduction of high-frequency voltage transitions in the terminal

TABLE II
VALUES OF COMMON-MODE VOLTAGE AND POLE VOLTAGES FOR CORRESPONDING OUTPUT VOLTAGE

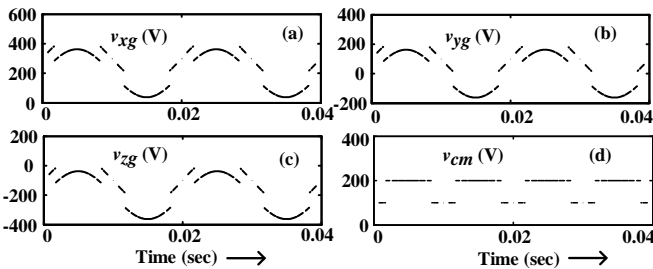| v_{uv}	v_{uz}	v_{vz}	v_{cm}
$+V_{PV}$	V_{PV}	0	$V_{PV}/2$
$+V_{PV}/2$	$V_{PV}/2$	0	$V_{PV}/4$
0	undefined	undefined	undefined
$-V_{PV}/2$	0	$V_{PV}/2$	$V_{PV}/4$
$-V_{PV}$	0	V_{PV}	$V_{PV}/2$

Fig. 7. The analytical results of proposed five-level CMLI showing the waveforms of: (a) terminal voltage v_{xg}; (b) terminal voltage v_{yg}; (c) terminal voltage v_{zg}; (d) common-mode voltage v_{cm}.

voltage further helps in reducing the leakage current in the PV system. The PV array parasitic capacitance [18] offers a high impedance for the low-frequency transitions in the terminal voltage. Thus, the magnitude of leakage current flowing through the parasitic capacitance is less. In other words, the proposed PWM technique minimizes the leakage current by reducing the high-frequency transitions in the terminal and common-mode voltages.

VI. SIMULATION RESULTS

To support the switching function analysis given in the previous section, the proposed five-level CMLI is simulated using POWERSIM blocks in the MATLAB/SIMULINK software. The PWM technique explained in section III is used for the proposed five-level CMLI configuration. Table III gives the value of various parameters used for simulating the proposed five-level CMLI. The proposed five-level CMLI needs to generate a voltage V_{inv} having a phase δ_{inv} [16] to feed the required amount of active power P into the grid.

TABLE III
PARAMETERS CONSIDERED FOR THE SIMULATION OF PROPOSED FIVE-LEVEL CMLI

Parameter	P	V_{DC}	f_{sw}	v_{ac}	f_{ac}
Value	2.5kW	400V	25kHz	220V	50Hz
Parameter	L_{ac}	R_{ac}	R_g	L_i	C_f
Value	4mH	0.01Ω	0.1Ω	4mH	0.1 μF
Parameter	R_d	C_p	R_p		
Value	50mΩ	200nF	1Ω		

$$\delta_{inv} = \arctan\left(\frac{2\Pi f_{ac}\left(L_{ac} + L_i\right)P}{v_{ac}^2 + R_{ac}P} \right)$$

(22)

$$V_{inv} = \left(v_{ac} + \frac{R_{ac}P}{v_{ac}} \right) \frac{1}{\cos \delta_{inv}}$$

(23)

For a power of P =2.5kW, the value of δ_{inv} = 0.117 rad and V_{inv} = 323 V are calculated by substituting the parameters from Table III in (22) and (23) respectively. The simulation waveforms of proposed five-level CMLI using the proposed PWM technique are shown in Fig. 8. Fig. 8(a) shows the output voltage of five-level CMLI. The presence of zero voltage state in all the voltage transitions of v_{uv} can be clearly noticed from the plot. The grid current i_{ac} is shown in Fig. 8(b). The grid current is nearly sinusoidal. The Total Harmonic Distortion (THD) of grid current i_{ac} is around 1.76% and meets the requirement of standard IEEE 1547.

The waveform of terminal voltages v_{xg}, v_{yg} and v_{zg} are shown in subplots (c), (d) and (e) of Fig. 8 respectively. The crucial observation made from these subplots is the absence of high-frequency voltage transitions. Also, these waveforms match with the result obtained using switching function analysis (Fig. 7). This justifies the analysis given in the previous section. Fig. 8(f) shows the waveform for leakage current i_{leak} flowing through the parasitic capacitor. The proposed PWM technique reduces the value of leakage current as can be observed in Fig. 8(f). This is because of the low-frequency voltage transitions in the terminal voltages v_{xg}, v_{yg} and v_{zg}. The spikes in the leakage current are observed when there is a sudden voltage transition in the terminal voltage. The

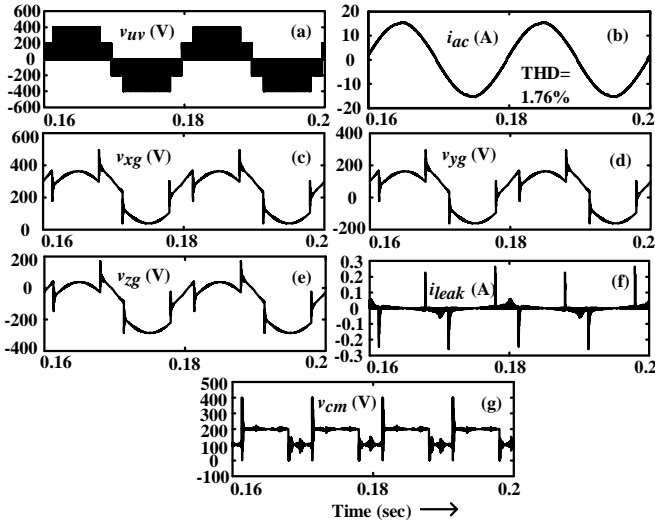Fig. 8. Simulation results of proposed five-level CMLI showing the waveforms of : (a) output voltage v_{uv}; (b) grid current i_{ac}; (c) terminal voltage v_{xg}; (d) terminal voltage v_{yg}; (e) terminal voltage v_{zg}; (f) leakage current i_{leak}; (g) common-mode voltage v_{cm}.

RMS value of i_{leak} is less than 20mA which is as per the standard VDE0126-1-1[13]. Fig. 8(g) shows the waveform of common-mode voltage v_{cm}. The high-frequency voltage transitions in the common-mode voltage are also avoided. This further brings down the size, weight and cost of the EMI filter to be used in the grid-connected system [22].

Another simulation is carried out with the proposed configuration to demonstrate the MPPT operation. The proposed five-level CMLI is operated using two MPPT algorithms to extract the maximum power from the individual PV arrays. As explained in section IV, the two individual MPPT algorithms are used for the two PV sources PV_1 and PV_2 which are identical (having same array configuration). Simulation is done considering a resistive load connected to the output of the inverter *via* an LC filter. The PV modules with an open circuit voltage of 21.05V and short circuit current of 3.74A at STC are chosen for the array simulation. The electrolytic capacitors of 5000μF are used as a buffer between the PV sources and inverter as shown in Fig. 1. The inverter is connected to a load of 20Ω through an LC filter with the inductor and capacitor values of 4mH and 2μF respectively. The two PV arrays PV_1 and PV_2 have an open circuit voltage of 126.90V and a short circuit current of 3.8A at an insolation of 1.0 Sun and the temperature of 50°C.

Fig. 9 shows the simulation results of MPPT performance for the proposed five-level CMLI. The subplots (Figs. 9(a) and Fig. 9(b)) show the waveforms of PV voltages V_{PV1} and V_{PV2} for PV_1 and PV_2 sources respectively. The values of the operating voltages V_{PV1} and V_{PV2} of the two PV arrays are nearly equal. The PV currents I_{PV1} and I_{PV2} are shown in subplots Fig. 9(c) and Fig. 9(d) respectively. The voltage-current (*v-i*) characteristics of the PV array can be observed with the increasing value of current by decreasing voltage or vice-versa. The power P_{PV1} and P_{PV2} from the PV sources PV_1 and PV_2 are shown in subplots Fig. 9(e) and Fig. 9(f) respectively. The operation of two PV sources near MPP can be confirmed with the low value of ripple in the PV power and

small oscillations in the modulation index m_a, which can be observed in zoomed part of Fig. 9(g). The waveform of output power across resistive load P_{load} is shown in subplot Fig. 9(h). It can be observed that the power across output load is nearly equal to the sum of the individual PV powers P_{PV1} and P_{PV2}. The waveforms of $v_{ref\_modified}$ and v_{uv} are also shown in subplots Fig. 9(i) and Fig. 9(j). Integration of MPPT for the proposed five-level CMLI makes the inverter suitable for the PV systems.

VII. EXPERIMENTAL RESULTS

To validate the analysis and simulation of PWM technique for the given five-level CMLI, an experimental setup is established. Fig. 10 shows the photograph of the fabricated experimental setup. The details of the parameters used for the experiment are given in Table IV. The MOSFET's with part number IRF840 are employed as switches in the power circuit. The driving pulses for the switches are generated using HCPL 3120. The programmable dc power supplies give the input DC voltage V_{DC} to the inverter [8, 23-25] as shown in Fig. 10. The output of the inverter is connected to a resistive load R_{load} through an LC filter. The required PWM pulses are generated using DIGILENT ATLYS Spartran-6 FPGA board. The frequency of carrier wave f_{sw} and the modified reference wave f_r are selected as 10kHz and 50Hz respectively. The measurement of leakage current is done by connecting a capacitor C_p in series with resistance R_p at point x of the given five-level inverter as shown in Fig. 1.

Fig. 11 shows the experimental waveforms of the proposed five-level CMLI. Fig. 11(a) shows the waveform of switching states of switches S_{x1}, S_{x3}, S_{x4}, S_{x5}, S_{x6} and S_{x7}. The switches (S_{x1}, S_{x2}) and (S_{x7}, S_{x8}) are operated at low switching
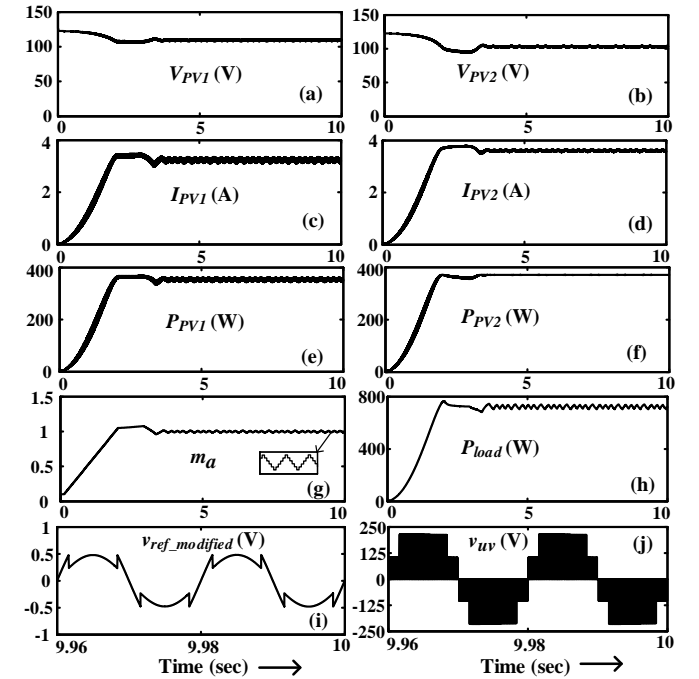

Fig. 9. Proposed five-level CMLI integrated with MPPT. The subplots give waveforms of : (a) voltage V_{PV1}; (b) voltage V_{PV2}; (c) current I_{PV1}; (d) current I_{PV2}; (e) power P_{PV1}; (f) power P_{PV2}; (g) resultant modulation index m_a; (h) output power P_{OUT}; (i) modified reference wave $v_{ref\_modified}$; (j) inverter output voltage v_{ab}.
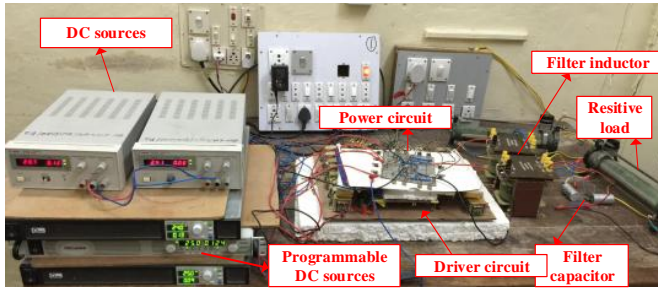
Fig. 10. Photograph of the experimental setup containing five-level and nine-level CMLI.

TABLE IV
PARAMETERS USED FOR EXPERIMENTAL SETUP

Parameter	P	V_{DC}	f_{sw}	f_{ac}	L
Value	54W	220V	10kHz	50Hz	4mH
Parameter	C	R_{load}	C_p	R_p	
Value	1.25µF	370 Ω	200nF	5Ω	

frequency. The remaining switches (S_{x3}, S_{x6}) and (S_{x4}, S_{x5}) operate only in positive and negative half cycles of the inverter output voltage v_{uv} respectively. The inverter output voltage v_{uv} is shown in Fig. 11(b). The zero voltage state is present in all the switchings of the inverter output voltage. This may increase the filter inductor value at the output of MLI. However, the minimization of high-frequency transitions in the terminal voltage reduces EMI filter requirement for the proposed system. The waveforms of the voltage across resistive load v_{load} and the current flowing through the resistive load i_{load} are shown in Fig. 11(c). The waveforms of the terminal voltages v_{xg}, v_{yg} and v_{zg} are shown in Fig. 11(d). It may be noted that the terminal voltage is free from high-frequency transitions, which demonstrates the effectiveness of the proposed PWM technique. Fig. 11(e) shows the leakage current i_{leak} flowing through the C_p-R_p branch. The magnitude of leakage current is less than 100mA and is as per standard VDE0126-1-1.

To demonstrate the upgradability of the proposed topology to any generalized $2m+1$ level inverter, a hardware prototype for the nine-level CMLI is fabricated. The nine-level configuration of proposed CMLI is obtained by cascading two basic units in generalized configuration with the bi-directional switches as shown in Fig. 4. Fig. 12 shows the experimental waveforms obtained from the developed hardware prototype of the nine-level inverter connected to a resistive load. The parameters shown in Table IV are again used, except the input DC voltage which is reduced to 100V. Fig. 12(a) shows the waveform of inverter output voltage v_{uv}. The nine levels of the inverter output voltage can be clearly observed in the voltage waveform. The presence of zero voltage state for a complete cycle of the output voltage is also observed from the plot. The waveforms of the voltage across the resistive load v_{load} and the current flowing through resistive load i_{load} are shown in Fig. 12(b).

VIII. COMPARISON OF PROPOSED CMLI WITH THE EXISTING MLI TOPOLOGIES

The proposed five-level CMLI is compared with the existing PV MLI topologies from the literature available. Table V gives the comparison details of the proposed five-level
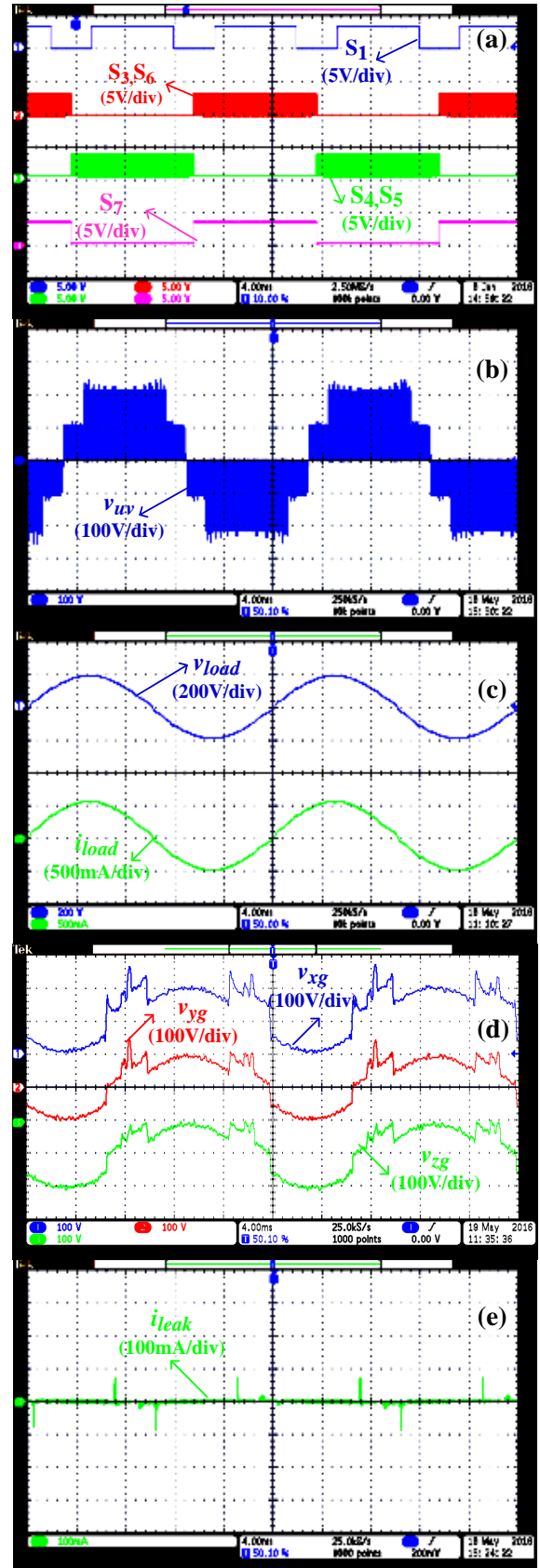

Fig. 11. The experimental waveforms of : (a) switching functions of switches S_{x1}, S_{x3}, S_{x4}, S_{x5}, S_{x6}, S_{x7}; (b) output voltage v_{uv}; (c) voltage v_{load} across and current i_{load} flowing through resistive load; (d) terminal voltage waveforms of v_{xg}, v_{yg} and v_{zg}; (e) leakage current i_{leak} in the parasitic capacitance for the proposed five-level CMLI.
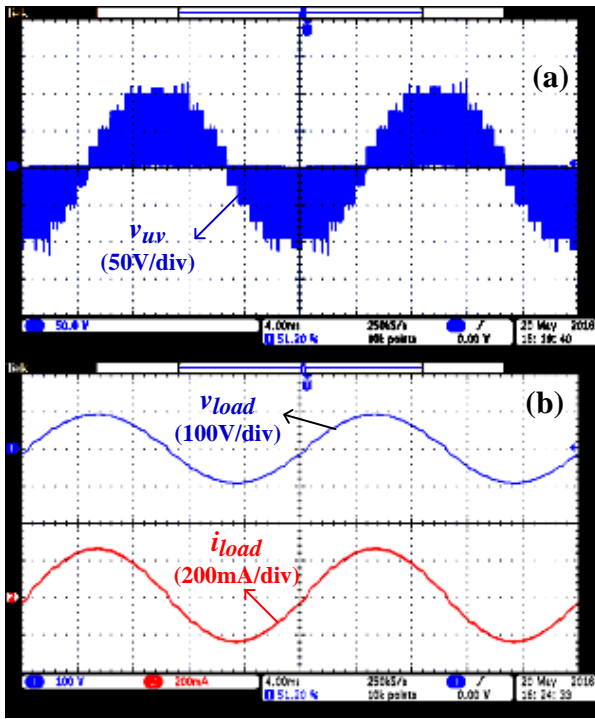
Fig. 12. The experimental waveforms of nine-level CMLI : (a) output voltage v_{uv}; (b) voltage v_{load} across and current i_{load} flowing through the resistive load.

CMLI with the existing PV MLI topologies. It can be observed that the other topologies (Table V) require almost the same number of devices for the generation of three levels in the output voltage. The proposed CMLI also requires nearly the same number of semiconductor devices for the generation of five levels in the inverter output voltage. Hence, the proposed five-level CMLI is economical. Furthermore, the proposed five-level CMLI have reduced switching and conduction losses. The other existing topologies shown in Table V have either high switching loss or conduction loss. The problem of asymmetry in the output voltage of the inverter is also avoided in the proposed CMLI topology. Also, the number of devices conducting during zero voltage state always remains two. Thus, the proposed CMLI is expected to show high efficiency. To support the efficient operation of proposed CMLI, loss calculation (switching and conduction losses) for the controlled switching devices is done under identical conditions. The losses in other MLI topologies are also calculated under the same conditions of output power P=2.5kW, switching frequency f_{sw}=25kHz, V_{DC}=400V and m_a=0.8125. The expressions for switching and conduction losses used for the calculation are obtained from [12] and [28]. Fig. 13 and Fig. 14 show the calculated value of conduction and switching losses in the form of bar charts for various MLI topologies reported in the literature. Furthermore, in Figs. 13 and 14, the terms P_c and P_{sw} refer to the conduction and switching losses respectively, for each of the MLI topologies reported in the literature. Conduction and switching losses of the individual switches in each MLI topology are shown in different color blocks in the bar chart of P_c and P_{sw} respectively. It can be observed that the proposed five-level CMLI shows higher efficiency compared to the other existing topologies. Hence,

TABLE V
COMPARISON OF PROPOSED CMLI WITH THE EXISTING TOPOLOGIES

S.No	Author name [Ref no], number of levels in output voltage	A	B	C		D		E		F	
				s	d	p	n	p	n	p	n
1	Zhang et al. [9], 3-L	Yes	4	8	-	4	2	2	2	2	2
2	Islam et al [10], 3-L	No	2	6	-	3	3	3	3	1	1
3	Xiao et al. [11], 3-L	No	2	6	4	2	2	4	4	0	0
4	Ji et al. [12], 3-L	No	2	6	2	3	3	2	2	1	1
5	Kerekes et al [23], 3-L	No	3	5	5	2	2	3	3	0	0
6	Islam et al [26], 3-L	Yes	2	7	3	2	3	3	3	1	1
7	Wu et al [27], 3-L (HBI MODE)	Yes	4	9	6	6	6	4	4	0	0
8	Wu et al [27], 5-L (CHI MODE)	No	4	8	2	6	6	8	8	0	0
9	Proposed 5-LCMLI	No	2	8	-	3	3	2	2	3	3

A- Asymmetry operation during positive and negative cycle of the MLI;
B- Number of devices conducting in zero voltage state including switches and diodes;
C- Number of devices used in the MLI:
   s- Number of switches used in the MLI;
   d- Number of diodes used in the MLI;
D- Number of devices including switches and diodes conducting:
   p- During the positive half-cycle of the grid voltage;
   n- During the negative half-cycle of the grid voltage;
E- Number of switches operating at high switching frequency;
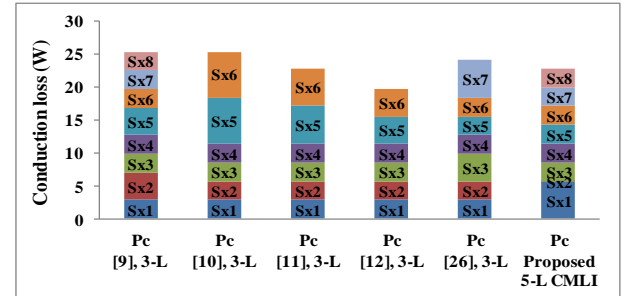F- Number of switches operating at low switching frequency;

Fig. 13. The value of conduction losses P_c of switches used in various MLI topologies given in the literature.
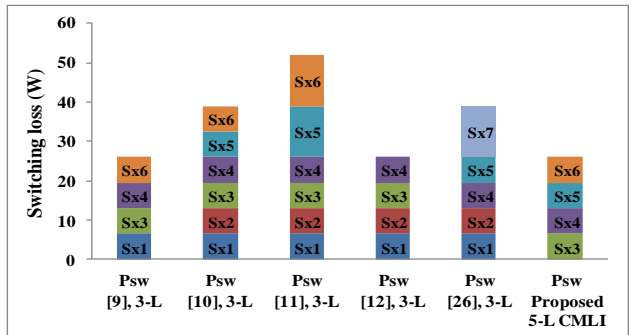

Fig. 14. The value of switching loss P_{sw} of switches used in various MLI topologies presented in the literature.

the proposed five-level CMLI is efficient and economical.

IX. CONCLUSION

In this paper, an improved five-level CMLI with low switch count for the minimization of leakage current in a transformerless PV system is proposed. The proposed CMLI minimizes the leakage current by eliminating the high-frequency transitions in the terminal and common-mode

voltages. The proposed topology also has reduced conduction and switching losses which makes it possible to operate the CMLI at high switching frequency. Furthermore, the solution for generalized $2m+1$ levels CMLI is also presented in the paper. The given PWM technique requires only one carrier wave for the generation of $2m+1$ levels. The operation, analysis of terminal and common-mode voltages for the CMLI is also presented in the paper. The simulation and experimental results validate the analysis carried out in this paper. The MPPT algorithm is also integrated with the proposed five-level CMLI to extract the maximum power from the PV panels. The proposed CMLI is also compared with the other existing MLI topologies in Table V to show its advantages.

REFERENCES

[1] Y. Tang, W. Yao, P.C. Loh and F. Blaabjerg, "Highly Reliable Transformerless Photovoltaic Inverters With Leakage Current and Pulsating Power Elimination," *IEEE Trans. Ind. Elect*., vol. 63, no. 2, pp. 1016-1026, Feb. 2016.

[2] W. Li, Y. Gu, H. Luo, W. Cui, X. He and C. Xia, "Topology Review and Derivation Methodology of Single-Phase Transformerless Photovoltaic Inverters for Leakage Current Suppression," *IEEE Trans. Ind. Elect*., vol. 62, no. 7, pp. 4537-4551, July 2015.

[3] J. Ji, W. Wu, Y. He, Z. Lin, F. Blaabjerg and H. S. H. Chung, "A Simple Differential Mode EMI Suppressor for the LLCL-Filter-Based Single-Phase Grid-Tied Transformerless Inverter," *IEEE Trans. Ind. Elect*., vol. 62, no. 7, pp. 4141-4147, July 2015.

[4] Y. Bae and R.Y.Kim, "Suppression of Common-Mode Voltage Using a Multicentral Photovoltaic Inverter Topology With Synchronized PWM," *IEEE Trans. Ind. Elect*., vol. 61, no. 9, pp. 4722-4733, Sept. 2014.

[5] N. Vazquez, M. Rosas, C. Hernandez, E. Vazquez and F. J. Perez-Pinal, "A New Common-Mode Transformerless Photovoltaic Inverter," *IEEE Trans. Ind. Elect*., vol. 62, no. 10, pp. 6381-6391, Oct. 2015.

[6] G. Buticchi, E. Lorenzani and G. Franceschini, "A Five-Level Single-Phase Grid-Connected Converter for Renewable Distributed Systems," *IEEE Trans. Ind. Elect*., vol.60, no.3, pp.906-918, March 2013.

[7] N.A. Rahim and J. Selvaraj, "Multistring Five-Level Inverter With Novel PWM Control Scheme for PV Application," *IEEE Trans. Ind. Elect*., vol.57, no.6, pp.2111-2123, June 2010.

[8] M. Cavalcanti, K. De Oliveira, A. M. de Farias, F. Neves, G. Azevedo and F. Camboim, "Modulation Techniques to Eliminate Leakage Currents in Transformerless Three-Phase Photovoltaic Systems," *IEEE Trans. Ind. Elect*., vol. 57, no. 4, pp. 1360-1368, April 2010.

[9] L. Zhang, K. Sun, L. Feng, H. Wu and Y. Xing, "A Family of Neutral Point Clamped Full-Bridge Topologies for Transformerless Photovoltaic Grid-Tied Inverters," *IEEE Trans. Power Elect*., vol.28, no.2, pp.730-739, Feb. 2013.

[10] M. Islam and S. Mekhilef, "H6-type transformerless single-phase inverter for grid-tied photovoltaic system," *IET Elect. Power Elect*., vol.8, no.4, pp.636-644, 2015.

[11] H.F. Xiao, K. Lan and L. Zhang, "A Quasi-Unipolar SPWM Full-Bridge Transformerless PV Grid-Connected Inverter with Constant Common-Mode Voltage," *IEEE Trans. Power Elect*., vol.30, no.6, pp.3122-3132, June 2015.

[12] B.Ji, J. Wang and J. Zhao, "High-Efficiency Single-Phase Transformerless PV H6 Inverter With Hybrid Modulation Method," *IEEE Trans. Ind. Elect*., vol.60, no.5, pp.2104-2115, May 2013.

[13] G. Buticchi, D. Barater, E. Lorenzani, C. Concari and G. Franceschini, "A Nine-Level Grid-Connected Converter Topology for Single-Phase Transformerless PV Systems," *IEEE Trans. Ind. Elect*., vol.61, no.8, pp.3951-3960, Aug. 2014.

[14] F. Hong, J. Liu, B. Ji, Y. Zhou, J. Wang and C. Wang, "Single Inductor Dual Buck Full-Bridge Inverter," *IEEE Trans. Ind. Elect*., vol.62, no.8, pp.4869-4877, Aug. 2015.

[15] S. V. Araujo, P. Zacharias and R. Mallwitz, "Highly Efficient Single-Phase Transformerless Inverters for Grid-Connected Photovoltaic Systems," *IEEE Trans. Ind. Elect*., vol. 57, no. 9, pp. 3118-3128, Sept. 2010.

[16] O. Lopez, R. Teodorescu and J. D. Gandoy, "Multilevel transformerless topologies for single-phase grid-connected converters," APEC 2006, pp.5191-5196, Nov. 2006.

[17] O. Lopez, R. Teodorescu, F. Freijedo and J.D. Gandoy, "Leakage current evaluation of a single-phase Transformerless PV inverter connected to the grid," APEC 2007, pp.907-912, March 2007.

[18] O. Lopez, F.D. Freijedo, A.G. Yepes, P. F. Comesaa, J. Malvar, R. Teodorescu and J. D. Gandoy, "Eliminating Ground Current in a Transformerless Photovoltaic Application," *IEEE Trans. Energy Conv.*, vol.25, no.1, pp.140-147, March 2010.

[19] G. Vazquez, P.R.M. Rodriguez, G. Escobar, J.M. Sosa and R.M. Mendez, "A PWM method for single-phase cascade multilevel inverters to reduce leakage ground current in transformerless PV systems," (accepted for publication in International Transactions on Electrical Energy Systems, Wiley Publications).

[20] M. Killi and S. Samanta, "Modified Perturb and Observe MPPT Algorithm for Drift Avoidance in Photovoltaic Systems," *IEEE Trans. Ind. Elect*., vol. 62, no. 9, pp. 5549-5559, Sept. 2015.

[21] M. Hedayati and V. John, "Filter Configuration and PWM Method For Single Phase Inverters with Reduced Conducted EMI Noise," *IEEE Trans. Ind. App*., vol. 51, no. 4, pp. 3236-3243, July-Aug. 2015.

[22] D. Barater, G. Buticchi, E. Lorenzani and C. Concari, "Active Common-Mode Filter for Ground Leakage Current Reduction in Grid-Connected PV Converters Operating With Arbitrary Power Factor," *IEEE Trans. Ind. Elect*., vol.61, no.8, pp.3940-3950, Aug. 2014.

[23] T. Kerekes, R. Teodorescu, P. Rodriguez, G. Vazquez and E. Aldabas, "A New High-Efficiency Single-Phase Transformerless PV Inverter Topology," *IEEE Trans. Ind. Elect*., vol.58, no.1, pp.184-191, Jan. 2011.

[24] T. Kerekes, R. Teodorescu, M. Liserre, C. Klumpner and M. Sumner, "Evaluation of Three-Phase Transformerless Photovoltaic Inverter Topologies," *IEEE Trans. Power Elect*., vol. 24, no. 9, pp. 2202-2211, Sept. 2009.

[25] T. K. S. Freddy, N. A. Rahim, W. P. Hew and H. S. Che, "Modulation Techniques to Reduce Leakage Current in Three-Phase Transformerless H7 Photovoltaic Inverter," *IEEE Trans. Ind. Elect*., vol. 62, no. 1, pp. 322-331, Jan. 2015.

[26] M. Islam and S. Mekhilef, "Efficient Transformerless MOSFET Inverter for Grid-Tied Photovoltaic System," *IEEE Trans. Power Elect.,* vol. 31, no. 9, pp. 6305-6316, Sept. 2016.

[27] F. Wu, X. Li, F. Feng and H.B.Gooi, "Modified Cascaded Multilevel Grid-Connected Inverter to Enhance European Efficiency and Several Extended Topologies," *IEEE Trans. Ind. Elect*., vol. 11, no. 6, pp. 1358-1365, Oct. 2013.

[28] S. Clemente, "A simple tool for the selection of IGBTs for motor drives and UPSs," APEC 1995, pp. 755–764, TX, Mar.1995.

Sachin Jain (SM'16) is currently working as an Assistant Professor at the National Institute of Technology (NITW), Warangal, India. Before joining NIT-W, he was working as an Senior Design Engineer in the R&D Department of the Solar Energy Business Group of Schneider Electric at Bangalore. His research interests include power electronics applications in nonconventional energy conditioning, power quality, and distributed generation.

Venu Sonti (S'15) received B.Tech degree in Electrical and Electronics Engineering from the Koneru Lakshmaiah College of Engineering, Guntur, India in year 2011 and M.Tech degree in Power Electronics and Drives from the National Institute of Technology Warangal, Warangal, India in the year 2013. Currently, he is pursuing the Ph.D. degree from National Institute of Technology Warangal, India. His research interests include the grid-connected inverter for renewable energy generation.